Title	$\Lambda\Lambda$ interaction from relativistic heavy-ion collisions
Author(s)	Morita, Kenji; Furumoto, Takenori; Ohnishi, Akira
Citation	Physical Review C (2015), 91(2)
Issue Date	2015-02
URL	http://hdl.handle.net/2433/233191
Right	©2015 American Physical Society
Type	Journal Article
Textversion	publisher

PHYSICAL REVIEW C **91**, 024916 (2015)

$\Lambda\Lambda$ interaction from relativistic heavy-ion collisions

Kenji Morita,[1,2,3,*] Takenori Furumoto,[4] and Akira Ohnishi[1,†]

[1]*Yukawa Institute for Theoretical Physics, Kyoto University, Kyoto 606-8502, Japan*

[2]*Frankfurt Institute for Advanced Studies, Ruth-Moufang-Strasse 1, D-60438 Frankfurt am Main, Germany*

[3]*Institute of Theoretical Physics, University of Wroclaw, PL-50204 Wrocław, Poland*

[4]*National Institute of Technology, Ichinoseki College, Ichinoseki, Iwate 021-8511, Japan*

(Received 29 August 2014; revised manuscript received 27 January 2015; published 26 February 2015)

We investigate the two-particle intensity correlation function of Λ in relativistic heavy-ion collisions. We find that the behavior of the $\Lambda\Lambda$ correlation function at small relative momenta is fairly sensitive to the interaction potential and collective flows. By comparing the results of different source functions and potentials, we explore the effect of intrinsic collective motions on the correlation function. We find that the recent STAR data give a strong constraint on the scattering length and effective range of $\Lambda\Lambda$ interaction, as $-1.8\ \mathrm{fm}^{-1} < 1/a_0 < -0.8\ \mathrm{fm}^{-1}$ and $3.5\ \mathrm{fm} < r_{\mathrm{eff}} < 7\ \mathrm{fm}$, respectively, if Λ samples do not include the feed-down contribution from long-lived particles. We find that the feed-down correction for Σ^0 decay reduces the sensitivity of the correlation function to the detail of the $\Lambda\Lambda$ interaction. As a result, we obtain a weaker constraint, $1/a_0 < -0.8\ \mathrm{fm}^{-1}$. Implication for the signal of existence of H-dibaryon is discussed. Comparison with the scattering parameters obtained from the double Λ hypernucleus may reveal in-medium effects in the $\Lambda\Lambda$ interaction.

DOI: 10.1103/PhysRevC.91.024916 PACS number(s): 25.75.Gz, 21.30.Fe, 13.75.−n

I. INTRODUCTION

Hyperon-hyperon interaction plays an important role in various aspects of modern nuclear physics such as hypernuclear, exotic particle, neutron star, and strange matter physics. Current most precise information on $\Lambda\Lambda$ interaction is obtained from the double Λ hypernuclear mass [1–3], and it is closely related to the existence of the $S = -2$ dibaryon (the H particle). In the neutron star core, hyperons have been believed to emerge and to soften the equation of state [4]. While recent observation of massive neutron stars disfavors admixture of strange hadrons [5], hypernuclear physics data suggest hyperon admixture at $\rho_B = (2-4)\rho_0$ [4]. Deeper understanding of hyperon-hyperon interaction may help in solving this massive neutron star puzzle. At very high densities, hyperon superfluid could be continuously connected to the color superconductor, where the three flavors (uds) and colors (rgb) are entangled.

The existence of the H particle has been one of the long-standing problems in hadron physics. In 1977, Jaffe pointed out that double strange dibaryon made of six quarks ($uuddss$) may be deeply bound below the $\Lambda\Lambda$ threshold due to the strong attraction from color magnetic interaction based on the bag model calculation [6]. Deeply bound H was ruled out by the existence of double Λ hypernuclei. A double Λ hypernucleus ${}^{6}_{\Lambda\Lambda}\mathrm{He}$ was found to decay weakly (Nagara event), and the observed energy of ${}^{6}_{\Lambda\Lambda}\mathrm{He}$ is 7.25 MeV($=B_{\Lambda\Lambda}$) below the ${}^{4}\mathrm{He} + \Lambda\Lambda$ threshold [1]. Since ${}^{6}_{\Lambda\Lambda}\mathrm{He}$ should decay to ${}^{4}\mathrm{He} + H$ if the mass of H is $M_H < 2M_\Lambda - B_{\Lambda\Lambda}$, the deeply bound H was ruled out.

The H particle is again attracting much attention due to recent theoretical and experimental efforts. Recent lattice QCD calculations have demonstrated that H appears as the bound state around the flavor SU(3) limit, and they also suggest the possibility for H to appear as a bound state or resonance pole [7]. Experimentally, KEK-E224 and KEK-E522 experiments [8,9] demonstrated that the $\Lambda\Lambda$ invariant mass spectrum is enhanced in the low energy region between $\Lambda\Lambda$ and ΞN thresholds, compared with the phase space estimate and the classical transport model calculations [10]. Enhancement of the invariant mass spectrum just above the threshold implies the final state interaction effects of $\Lambda\Lambda$ attraction. KEK-E522 data also show the bump structure around 10 MeV above the $\Lambda\Lambda$ threshold. This bump cannot be explained solely by the final state interaction effects, but it is not significant enough ($\sim 2\sigma$) to claim the existence of a resonance pole [9].

It is evident that we need higher statistics data to obtain more precise information on $\Lambda\Lambda$ interaction, and eventually to conclude the existence/nonexistence of the H pole. Higher statistics data will be available from the future J-PARC experiments on double Λ hypernuclear observation and $\Lambda\Lambda$ invariant mass measurement, as proposed in the J-PARC E42 experiment. Recently, an alternative possibility to access the information on hadron-hadron interactions has been explored in heavy-ion collisions at the Relativistic Heavy Ion Collider (RHIC) and the Large Hadron Collider (LHC). The large hadron multiplicity, which is achieved by hadronization from the quark-gluon plasma (QGP), makes it possible to look at correlations between hadrons with good experimental statistics. In particular, the intensity correlation of identical particles in relative momentum space is known as the Hanbury-Brown and Twiss (HBT) or Goldhaber-Goldhaber-Lee-Pais (GGLP) effect to give information on the size of the emission source through the (anti)symmetrization of the two-boson (fermion) wave function.

The HBT effect of stable hadrons, particularly pions, has been used to estimate the source sizes created in relativistic nucleus-nucleus collisions. On the one hand, effects of interaction between two of those emitted particles on extracting

*kmorita@yukawa.kyoto-u.ac.jp

†ohnishi@yukawa.kyoto-u.ac.jp

source size can be absorbed into the chaoticity parameter, when the system has a large size compared with the interaction range. On the other hand, one expects substantial effects of the interaction on the correlation function of identical particles of which interaction is sufficiently strong in the range comparable to the effective source size [11,12]. This implies that one may be able to use the correlation function to obtain information on the interaction between two identical particles, even if those particles are unstable. For the $\Lambda\Lambda$ pair, this idea is not new. It was proposed in the 1980s that we can fix resonance parameters, when the source size is small [13]. The correlation at low relative momenta was proposed to be useful to discriminate the sign of the scattering length a_0, provided that the source size is large [14]; when $\Lambda\Lambda$ has a bound state ($a_0 > 0$), the scattering wave function must have a node at $r \simeq a_0$ in order to be orthogonal to the bound state wave function; then we may find the suppression of the correlation. The vertex detectors at RHIC have enabled us to really obtain the $\Lambda\Lambda$ correlation data in heavy-ion collisions with a good signal-to-noise ratio by choosing weakly decaying Λ off the reaction point [15,16].

In this paper, along with the above expectation, we investigate the interaction between two Λ baryons. Several hyperon-nucleon (YN) and hyperon-hyperon (YY) interaction models have been proposed so far by constraining parameters from a limited number of YN scattering experiments, flavor symmetries, and hypernuclear data. We calculate the $\Lambda\Lambda$ correlation functions with those interaction potentials. Given a model source function relevant for Au+Au collisions at $\sqrt{s_{NN}} = 200$ GeV, we discuss the modification of the correlation function due to the interaction and collective flow effects, then show that how the behavior the correlation function constrains the nature of the interaction. A preliminary report of the present work can be found in Ref. [17]. In this paper, we present a detailed systematic analysis with the updated experimental data of $\Lambda\Lambda$ correlation.

In Ref. [15], the STAR Collaboration has reported and analyzed their experimental data of $\Lambda\Lambda$ correlation with the Lednický and Lyuboshitz analytical model [11] which incorporates the effect of the $\Lambda\Lambda$ interaction in terms of the effective range and the scattering length together with the intercept (chaoticity) parameter λ and normalization as fitting parameters. Moreover, it has been shown that the inclusion of a residual correlation as an additional Gaussian term responsible for the high-momentum tail gives a better description of the data. In this paper, we focus on effects of the $\Lambda\Lambda$ interaction through the modification of the wave function and the deformation of the emission source function owing to the collective flow which takes place in relativistic heavy-ion collisions. We will show that the $\Lambda\Lambda$ correlation data measured by the STAR Collaboration including the intercept and the residual correlation can be explained with some of the recent $\Lambda\Lambda$ potentials and flow parameters constrained by the single particle spectrum of Λ, if we assume feed-down correction is negligible. We will then examine effects of Σ^0 feed-down correction on the obtained constraints and discuss their interplay with a residual correlation.

This paper is organized as follows. In Sec. II, we briefly summarize models of the $\Lambda\Lambda$ interaction. In Sec. III, we introduce the two-particle correlation function with the final state interaction and show the general property based on a simple source model. Intrinsic effects in relativistic heavy-ion collisions are discussed in Sec. IV. We discuss feed-down correction and residual correlations in Sec. V. We also discuss possible implications for the H particle in Sec. VI. Section VII is devoted to concluding remarks.

II. ΛΛ INTERACTION POTENTIAL

We examine several models of $\Lambda\Lambda$ interaction proposed so far by using $\Lambda\Lambda$ correlation in heavy-ion collisions. Since experimental information on $\Lambda\Lambda$ interaction is limited, $\Lambda\Lambda$ correlation data are useful to constrain $\Lambda\Lambda$ interaction. $\Lambda\Lambda$ interaction is known to be weakly attractive from the $\Lambda\Lambda$ bond energy in ${}^{6}_{\Lambda\Lambda}$He, $\Delta B_{\Lambda\Lambda} = B_{\Lambda\Lambda}({}^{6}_{\Lambda\Lambda}\mathrm{He}) - 2B_{\Lambda}({}^{5}_{\Lambda}\mathrm{He}) \simeq 1.01$ MeV [1]. From $\Delta B_{\Lambda\Lambda}({}^{6}_{\Lambda\Lambda}\mathrm{He})$, the scattering length and the effective range in the $\Lambda\Lambda$ ${}^1S_0$ channel are suggested as $(a_0, r_{\mathrm{eff}}) = (-0.77\ \mathrm{fm}, 6.59\ \mathrm{fm})$ [2] or $(a_0, r_{\mathrm{eff}}) = (-0.575\ \mathrm{fm}, 6.45\ \mathrm{fm})$ [3], but in principle one cannot determine two low energy scattering parameters from a single observed number of $\Delta B_{\Lambda\Lambda}$. For example, while r_{eff} values are very similar, a_0 are different by 25–30% in the above two estimates. Low energy $\Lambda\Lambda$ scattering parameters are useful to distinguish the models of baryon-baryon (BB) interaction. The long-range part of the NN interaction is dominated by the one-pion exchange potential, which roughly determines the low energy behavior of NN scattering. By comparison, the Λ particle is isoscalar and there is no one-pion exchange in $\Lambda\Lambda$ interaction. Thus the low energy $\Lambda\Lambda$ scattering parameters, such as the scattering length a_0 and the effective range r_{eff}, are more sensitive to the BB interaction models.

There are several types of $\Lambda\Lambda$ interactions proposed so far. Meson exchange model $\Lambda\Lambda$ interactions [18–23] have a long history of studies. The Nijmegen group has provided several versions of NN, YN, and YY interactions, model D (ND) [18], model F (NF) [19], soft core (NSC89 and NSC97) [20,21], and extended soft core (ESC08) [22]. These interactions have been widely used in hypernuclear structure calculations [2,3]. Compared with NN and YN interactions, we have larger uncertainties in YY interaction and there are some rooms to vary model parameters. We regard the hard core radius r_c in hard core models (ND and NF) and the cutoff mass m_{cut} in NSC89 as free parameters. In the case of NSC97, there are several versions (NSC97a-f) having different spin dependence in ΛN interaction, and $\Lambda\Lambda$ scattering parameters would help in discriminating these versions.

The Ehime potential is a boson exchange $\Lambda\Lambda$ potential [23], whose strength is fitted to the old double Λ hypernuclear bond energy, $\Delta B_{\Lambda\Lambda} = 4$ MeV [24]. Since this value is proven to be too large, the Ehime potential is now known to be too attractive. Even though, it would be valuable to examine the $\Lambda\Lambda$ correlation with more attractive potential than usually considered.

The quark model BB interactions have a merit that the Pauli principle between quarks and the one-gluon exchange give rise to the short range repulsion, which seems to be consistent with other NN interaction models. At the same time, in order to describe the medium- and long-range part of the BB

TABLE I. ΛΛ potentials. The scattering length (a_0) and effective range ($r_{\rm eff}$) are fitted using a two-range Gaussian potential, $V_{\Lambda\Lambda}(r) = V_1 \exp(-r^2/\mu_1^2) + V_2 \exp(-r^2/\mu_2^2)$.

Model	a_0 (fm)	$r_{\rm eff}$ (fm)	μ_1 (fm)	V_1 (MeV)	μ_2 (fm)	V_2 (MeV)	Ref.
ND46	4.621	1.300	1.0	−144.89	0.45	127.87	[18] $r_c = 0.46$ fm
ND48	14.394	1.633	1.0	−150.83	0.45	355.09	[18] $r_c = 0.48$ fm
ND50	−10.629	2.042	1.0	−151.54	0.45	587.21	[18] $r_c = 0.50$ fm
ND52	−3.483	2.592	1.0	−150.29	0.45	840.55	[18] $r_c = 0.52$ fm
ND54	−1.893	3.389	1.0	−147.65	0.45	1114.72	[18] $r_c = 0.54$ fm
ND56	−1.179	4.656	1.0	−144.26	0.45	1413.75	[18] $r_c = 0.56$ fm
ND58	−0.764	6.863	1.0	−137.74	0.45	1666.78	[18] $r_c = 0.58$ fm
NF42	3.659	0.975	0.6	−878.97	0.45	1048.58	[19] $r_c = 0.42$ fm
NF44	23.956	1.258	0.6	−1066.98	0.45	1646.65	[19] $r_c = 0.44$ fm
NF46	−3.960	1.721	0.6	−1327.26	0.45	2561.56	[19] $r_c = 0.46$ fm
NF48	−1.511	2.549	0.6	−1647.40	0.45	3888.96	[19] $r_c = 0.48$ fm
NF50	−0.772	4.271	0.6	−2007.35	0.45	5678.97	[19] $r_c = 0.50$ fm
NF52	−0.406	8.828	0.6	−2276.73	0.45	7415.56	[19] $r_c = 0.52$ fm
NSC89-1020	−0.250	7.200	1.0	−22.89	0.45	67.45	[20] $m_{\rm cut} = 1020$ MeV
NSC89-920	−2.100	1.900	0.6	−1080.35	0.45	2039.54	[20] $m_{\rm cut} = 920$ MeV
NSC89-820	−1.110	3.200	0.6	−1904.41	0.45	4996.93	[20] $m_{\rm cut} = 820$ MeV
NSC97a	−0.329	12.370	1.0	−69.45	0.45	653.86	[21]
NSC97b	−0.397	10.360	1.0	−78.42	0.45	741.76	[21]
NSC97c	−0.476	9.130	1.0	−91.80	0.45	914.67	[21]
NSC97d	−0.401	1.150	0.4	−445.77	0.30	373.64	[21]
NSC97e	−0.501	9.840	1.0	−110.45	0.45	1309.55	[21]
NSC97f	−0.350	16.330	1.0	−106.53	0.45	1469.33	[21]
Ehime	−4.21	2.41	1.0	−146.6	0.45	720.9	[23]
fss2	−0.81	3.99	0.92	−103.9	0.41	658.2	[25]
ESC08	−0.97	3.86	0.80	−293.66	0.45	1429.27	[22]

interaction, we need to take account of the meson exchange between quarks or baryons. There are several quark model BB interactions which include the meson exchange effects. We adopt here the fss2 model [25], as a typical quark model interaction. This interaction is constructed for the octet-octet BB interaction and describes the NN scattering data at a comparable precision to meson exchange potential models. For fss2, we use a phase-shift equivalent local potential in the two range Gaussian form [25], derived by using the inversion method based on supersymmetric quantum mechanics [26].

Low energy scattering parameters of the ΛΛ interactions considered here are summarized in Table I. In Fig. 1, we show the scattering parameters ($1/a_0$ and $r_{\rm eff}$) of the ΛΛ interactions under consideration. These scattering parameters characterize the low energy scattering phase shift in the so-called shape independent form as

$$k \cot \delta = -\frac{1}{a_0} + \frac{1}{2} r_{\rm eff} k^2 + \mathcal{O}(k^4). \quad (1)$$

For negatively large $1/a_0$, the attraction is weak and the phase shift rises slowly at low energy. When we go from left to right in the figure, the interaction becomes more attractive and a bound state appears when a_0 becomes positive. We have parametrized the boson exchange ΛΛ interactions, described above in two-range Gaussian potentials,

$$V_{\Lambda\Lambda}(r) = V_1 \exp\left(-r^2/\mu_1^2\right) + V_2 \exp\left(-r^2/\mu_2^2\right), \quad (2)$$

then fit the low energy scattering parameters, a_0 and $r_{\rm eff}$.

In addition to the ΛΛ potentials listed in Table I, we also examine the potentials used in Refs. [2] [by Filikhin and Gal (FG)] and [3] [by Hiyama, Kamimura, Motoba, Yamada, and Yamamoto (HKMYY)] with the three-range Gaussian fit given in those references. The parameters are summarized in Table II.

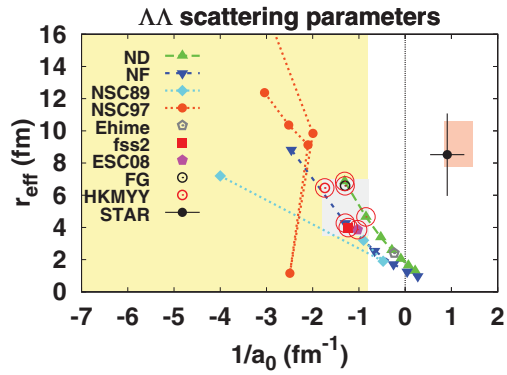

FIG. 1. (Color online) ΛΛ interactions and scattering parameters in the $(1/a_0, r_{\rm eff})$ plane. The ΛΛ interactions favored by the ΛΛ correlation data without feed-down correction are marked with big circles. The thin big and thick small shaded areas correspond to the favored regions of scattering parameters with and without feed-down correction, respectively, which show stable and small χ^2 minimum (see text). The results of the analysis by the STAR Collaboration is shown by the filled circle [15], together with systematic error represented by the surrounding shaded region.

TABLE II. $\Lambda\Lambda$ potentials from Nagara event. The scattering length (a_0) and effective range ($r_{\rm eff}$) are fitted using a three-range Gaussian potential, $V_{\Lambda\Lambda}(r) = V_1 \exp(-r^2/\mu_1^2) + V_2 \exp(-r^2/\mu_2^2) + V_3 \exp(-r^2/\mu_3^2)$.

Model	a_0 (fm)	$r_{\rm eff}$ (fm)	μ_1 (fm)	V_1 (MeV)	μ_2 (fm)	V_2 (MeV)	μ_3 (fm)	V_3 (MeV)	Ref.
HKMYY	−0.575	6.45	1.342	−10.96	0.777	−141.75	0.35	2136.6	[3]
FG	−0.77	6.59	1.342	−21.49	0.777	−250.13	0.35	9324.0	[2]

Before closing the section, we note that the coupling effects with ΞN and $\Sigma\Sigma$ channels are effectively incorporated in the present treatment, since the coupling modifies the low energy scattering parameters of $\Lambda\Lambda$ and we use the low energy phase shift equivalent potential. Also in Refs. [2,3], the coupling effects with ΞN is included in the $\Lambda\Lambda$ potential. The explicit coupling effect on the $\Lambda\Lambda$ correlation would be an interesting subject, but is out of the scope of this paper.

III. ΛΛ CORRELATION FUNCTION WITH INTERACTION EFFECTS

A. Formalism

A relevant formulation of the two-proton correlation function is given in [27] which solidates the formula in [28]. Here we apply the formula to $\Lambda\Lambda$ correlation. Then, for a given relative wave function Ψ_{12}, the correlation function defined as two-particle distribution $W_2(\boldsymbol{k_1},\boldsymbol{k_2})$ normalized by the one-particle distributions $W_1(\boldsymbol{k_i})(i = 1,2)$ can be expressed in terms of one-particle phase space density $S(x,\boldsymbol{k})$ as

$$C_2(\boldsymbol{Q},\boldsymbol{K}) = \frac{W_2(\boldsymbol{k_1},\boldsymbol{k_2})}{W_1(\boldsymbol{k_1})W_1(\boldsymbol{k_2})} \tag{3}$$

$$= \frac{\int d^4x_1 d^4x_2 S(x_1,\boldsymbol{K}) S(x_2,\boldsymbol{K}) |\Psi_{12}[\boldsymbol{Q},\boldsymbol{x_1}-\boldsymbol{x_2}-(t_2-t_1)\boldsymbol{K}/m]|^2}{\int d^4x_1 d^4x_2 S(x_1,\boldsymbol{k_1}) S(x_1,\boldsymbol{k_2})}, \tag{4}$$

where $\boldsymbol{K} = (\boldsymbol{k_1}+\boldsymbol{k_2})/2$ and $\boldsymbol{Q} = \boldsymbol{k_1}-\boldsymbol{k_2}$ are the average and the relative momentum of the two identical particles, respectively. Since the expression for the two-particle distribution is derived for small $\boldsymbol{Q}$, one can also put $\boldsymbol{k_1} \simeq \boldsymbol{k_2} \simeq \boldsymbol{K}$ in $S(x,\boldsymbol{k_i})$ in the denominator.

As $S(x,\boldsymbol{k})$ represents the one-particle phase space distribution of Λ, effects of interaction are embedded in the relative wave function $\Psi_{12}(\boldsymbol{Q},\boldsymbol{r})$. As we are considering the effect of $\Lambda\Lambda$ interaction through the potential $V(r)$, the relative wave function given by solving the Schrödinger equation is time independent. The factor $-(t_2-t_1)\boldsymbol{K}/m$, with m being the mass of Λ, is added to the relative coordinate in Ψ_{12} to take into account the different emission time of two Λ particles.

The two-particle wave function respects the antisymmetrization for the two identical fermions. For the noninteracting spin singlet (spin triplet) case, the spatial part of the wave function is symmetric (antisymmetric) with respect to the exchange of the two particle position,

$$\Psi_s = \frac{1}{\sqrt{2}}(e^{i\boldsymbol{k_1}\cdot\boldsymbol{x_1}+i\boldsymbol{k_2}\cdot\boldsymbol{x_2}} + e^{i\boldsymbol{k_2}\cdot\boldsymbol{x_1}+i\boldsymbol{k_1}\cdot\boldsymbol{x_2}})$$

$$= \frac{1}{\sqrt{2}} e^{2i\boldsymbol{K}\cdot\boldsymbol{X}}(e^{i\boldsymbol{Q}\cdot\boldsymbol{r}/2} + e^{-i\boldsymbol{Q}\cdot\boldsymbol{r}/2}), \tag{5}$$

$$\Psi_t = \frac{1}{\sqrt{2}}(e^{i\boldsymbol{k_1}\cdot\boldsymbol{x_1}+i\boldsymbol{k_2}\cdot\boldsymbol{x_2}} - e^{i\boldsymbol{k_2}\cdot\boldsymbol{x_1}+i\boldsymbol{k_1}\cdot\boldsymbol{x_2}})$$

$$= \frac{1}{\sqrt{2}} e^{2i\boldsymbol{K}\cdot\boldsymbol{X}}(e^{i\boldsymbol{Q}\cdot\boldsymbol{r}/2} - e^{-i\boldsymbol{Q}\cdot\boldsymbol{r}/2}), \tag{6}$$

where we have introduced the center-of-mass coordinate $\boldsymbol{X} = (\boldsymbol{x_1}+\boldsymbol{x_2})/2$ and relative one $\boldsymbol{r} = \boldsymbol{x_1}-\boldsymbol{x_2}$.

With the interaction described by a potential $V(r)$, we assume here that only the s wave is modified. The two-particle wave function in the spin singlet state is represented as, with the solution of the Schrödinger equation in the s-wave $\chi_Q(r)$,

$$\Psi_s = \sqrt{2}[\cos(\boldsymbol{Q}\cdot\boldsymbol{r}/2) + \chi_Q(r) - j_0(Qr/2)], \tag{7}$$

where $j_0(Qr/2)$ is the spherical Bessel function at zeroth order and we omit the $\boldsymbol{X}$ dependent part as they give unity in $|\Psi_{s,t}|^2$. The spin-averaged total wave function squared is now given by

$$|\Psi_{12}|^2 = \frac{1}{4}|\Psi_s|^2 + \frac{3}{4}|\Psi_t|^2 \tag{8}$$

$$= 1 - \frac{1}{2}\cos(\boldsymbol{Q}\cdot\boldsymbol{r}) + \left[\chi_Q(r) - j_0\left(\frac{Qr}{2}\right)\right] \times \cos\left(\frac{\boldsymbol{Q}\cdot\boldsymbol{r}}{2}\right) + \frac{1}{2}[\chi_Q(r) - j_0(Qr/2)]^2. \tag{9}$$

If we neglect the interaction $\chi_Q(r) = j_0(Qr/2)$, only the first and second terms remain to give the free HBT correlation which has an intercept $1/2$ at $\boldsymbol{Q} = 0$. This reflects symmetrization of the spatial wave function in the spin singlet channel and the antisymmetrization of the spatial wave function due to the Pauli principle in the spin triplet channel, $2 \times 1/4 + 0 \times 3/4 = 1/2$. On the other hand, it has been known that the bosonic correlation function gives the intercept value 2. Thus, we expect $C(\boldsymbol{Q} = 0) < 1/2$ for repulsive interactions and $C(\boldsymbol{Q} = 0) > 1/2$ for attractive ones.

Comparisons of the full correlation function with the free correlation function give direct information on the effect of the interaction, as we shall see below.

B. Static spherically symmetric source

In relativistic heavy-ion collisions, the source emitting hadrons shows collective behaviors. At the RHIC energy considered in this paper, the hot medium produced in the collisions exhibits a strongly correlated property which is understood as a nearly perfect fluid of the deconfined quarks and gluons. The hadrons are produced at the hadronization from the fluid, followed by rather dissipative transport processes [29]. As a result, the emission source $S(x,\boldsymbol{k})$ in Eq. (4) might not be characterized by a simple parametrization. In fact, the two-pion correlation functions have been extensively discussed in heavy-ion collisions and are found to be sensitive not only to the emission source size but to various aspects of the collision processes [30]. This fact made it difficult to fit the measured data within a simple model calculation even with collective effects being taken into account.

We expect that the Λ source may have a simpler form than that for pions for the following reasons. First, Λ is expected to interact weakly with environments mainly consisting of pions. Single particle levels of Λ including those of deep s states are clearly observed [31]. This is in contrast with nucleons and pions, whose single particle states have large widths inside nuclei, and suggests weaker interaction of Λ with pionic environment, since nuclei contain many virtual pions. Second, the decay feed effects are expected to be smaller. It is known that the feed-down effects of $\Lambda \to p\pi^-$ and $p\Lambda$ interactions are important to understand the pp correlation function. For the ΛΛ pair, there is no Coulomb suppression of low relative momentum pairs and contribution from particles which decay into Λ is limited. In addition, we can in principle remove those Λ particles from weak decays such as $\Xi^- \to \Lambda\pi^-$ by using the vertex detector. In the following, we will show that data on ΛΛ correlation measured in heavy-ion collisions at the RHIC energy are useful to discriminate the ΛΛ interaction.

To illustrate the capability, we first examine the correlation function from a simple, static, and spherically symmetric source

$$S_{\rm stat}(x,\boldsymbol{k}) = *\exp\left[-\frac{x^2+y^2+z^2}{2R^2}\right]\delta(t-t_0), \qquad (10)$$

where normalization is omitted since it is canceled in the correlation function.

Putting Eqs. (9) and (10) into Eq. (4) and projecting onto the function of $Q = |\boldsymbol{Q}|$ by integrating out the angle variables, the correlation function for the source function (10) becomes

$$C_{\rm stat}(Q) = 1 - \frac{1}{2}e^{-Q^2R^2} + \frac{1}{4\sqrt{\pi}R^3}\int_0^\infty dr\, r^2 e^{-r^2/4R^2} \times [[\chi_Q(r)]^2 - [j_0(Qr/2)]^2]. \qquad (11)$$

Thus the effect of interaction is incorporated as the difference of the squared relative wave function. The free case is given by a simple Gaussian, which is often used to obtain the source size.

In the static and spherically symmetric source model (10), the only parameter is the source size R. Thus, it is convenient to calculate

$$\chi^2 \equiv \sum_i \left[\frac{C(Q_i)^{\rm data} - C(Q_i)^{\rm model}}{\sigma_i^{\rm data}}\right]^2 \qquad (12)$$

as a function of R then search for minimum in order to address which potential is favored in data.

In the following, we compare the model correlation function (11) with the data of the ΛΛ correlation for $0.01 \leqslant Q_i < 0.5$ GeV, measured by the STAR Collaboration in Au+Au collisions at $\sqrt{s_{NN}} = 200$ GeV with 0–80% centrality [15]. χ^2 is calculated for all the potential tabulated in Tables I and II with the spherical static source model $S_{\rm stat}$.

The results are shown in Fig. 2, where $N_{\rm dof} = 24$. One sees that the behavior of $\chi^2/N_{\rm dof}$ as functions of R strongly depend on the choice of the potential. On the one hand, some potentials exhibit monotonically decreasing behavior with R then asympotically become flat. These potentials typically have too strong attraction (Ehime, ND50, NF46, ND46, NF44, etc.) or too large effective range (NSC97, NSC89). On the other hand, a stable minimum with small $\chi^2/N_{\rm dof}$ is achieved in the region 1 fm $< R <$ 1.5 fm in potentials such as ND56, NF50, fss2, and ESC08. Looking at the scattering length and the effective range of those potentials, we find that there is a range of those quantities in which the corresponding potentials show the stable and small χ^2 minimum, as shown in the shaded area in Fig. 1. There are also marginal potentials (HKMYY, NSC89-820) which exhibit also a stable minimum but with $\chi^2/N_{\rm dof} > 5$. Since we have compared with the raw data, these potentials may yield acceptable fit after appropriate corrections, thus should not be ruled out. NSC97d shows a different behavior from any other potentials, due to the narrow effective range and small scattering length as seen in Fig. 1 which may not be realistic. The small χ^2 at $R = 0.6$ fm is achieved by approaching the long tail part of $C(Q)$, rather than the interaction dominated part.

Figure 3 displays the correlation functions for potentials considered here compared with the experimental data. The size parameter R adopted in the figure corresponds to the minimum of χ^2 in Fig. 2. We also plot the free correlation function, Eq. (11) without the last term, for comparison. While the values of χ^2 do not differ much, the correlation function at low Q shows a substantial variation among the potentials. The small difference of χ^2 is attributed to larger error bars in the experimental data at low Q region. One sees that results from these potentials have all $C(Q) > 1/2$ at low Q, fairly reflecting the attraction between two Λ. Among the potentials with small minimum χ^2, on the one hand, NF50 and fss2 show $C(Q <$ 0.1 GeV$) \sim 0.9$ and give a good description for the tail part around $Q \sim 0.2$ GeV. On the other hand, ND56 and ESC08 exhibit a weak enhancement at $Q < 0.1$ GeV with a good fit to the data at 0.1 GeV $< Q <$ 0.3 GeV. Therefore, precision measurement at $Q < 0.1$ GeV will provide further constraints on the ΛΛ interaction. According to Table I, those potentials have -1.2 fm $< a_0 < -0.8$ fm and 3.2 fm $< r_{\rm eff} <$ 6.5 fm. However, the effective range is not constrained well because the model potentials do not have a combination of a large

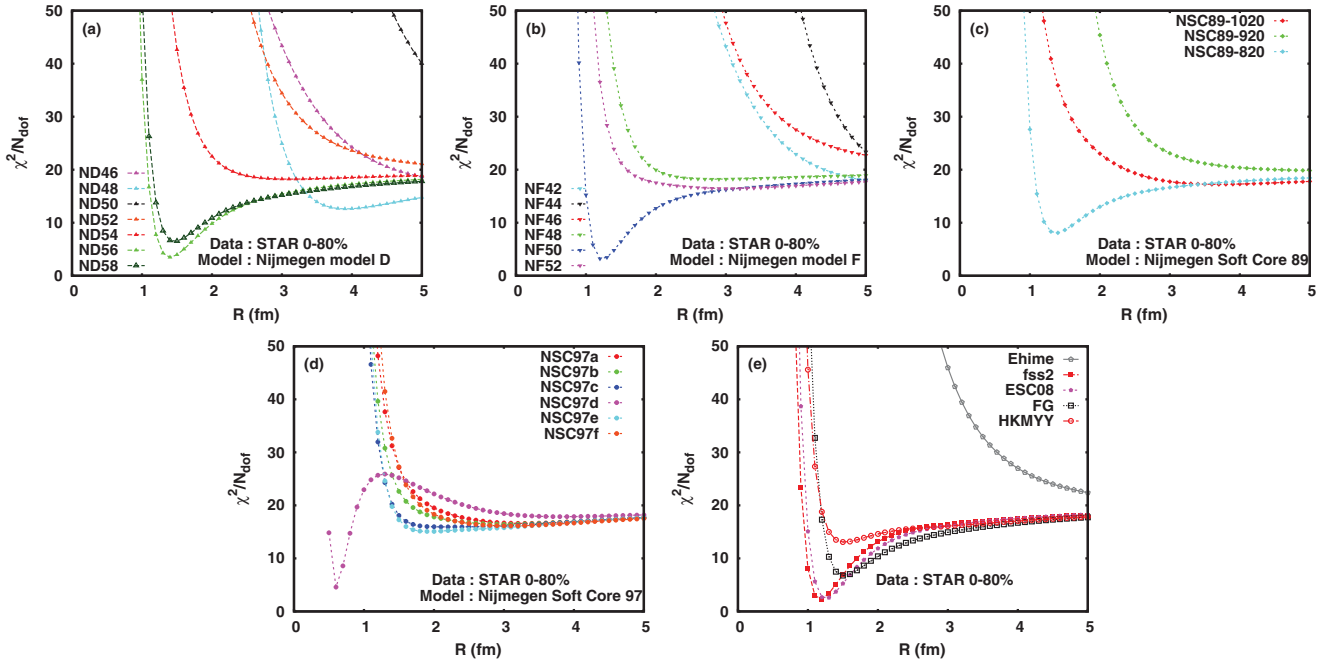

FIG. 2. (Color online) χ^2 plotted against R with $\Lambda\Lambda$ potentials. Nijmegen model D [ND, top left (a)], Nijmegen model F [NF, top middle (b)], Nijmegen soft core [NSC89, top right (c)], Nijmegen soft core [NSC97, bottom left (d)], and the rest of potentials in Tables I and II [bottom right (e)].

scattering length and a large effective range. Thus, we further construct model potentials by varying the effective range with a fixed scattering length $a_0 = -0.8$ fm in the two-range Gaussian (TRG) form (2). The parameter sets are summarized in Table III. Results for the $\chi^2/N_{\rm dof}$ and corresponding $C(Q)$ are displayed in Fig. 4. One sees that there always exists a minimum in the χ^2 plot which is particularly sensitive to variation of the effective range around $r_{\rm eff} \simeq 4$ fm. The global minimum achieved for $r_{\rm eff} \simeq 4$ fm is in accordance with the above model analysis. Since the behavior of $C(Q)$ with large effective range, $r_{\rm eff} > 6$ fm, is similar to FG and HKMYY in Fig. 3, a large effective range might be favored if the data receive the correction. Consequently, the present analysis provides rather more limited constraints on the effective range than the scattering length. The favored range of the scattering length and the effective range is indicated by the shaded area in Fig. 1.

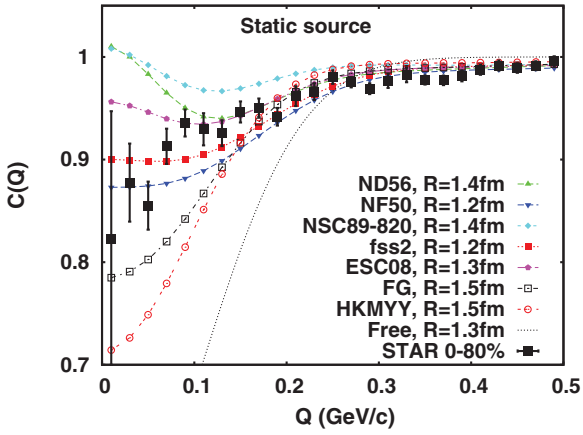

FIG. 3. (Color online) $\Lambda\Lambda$ correlation function from the static spherically symmetric source at the minimum of χ^2 together with experimental data by STAR.

C. Wave functions

In order to characterize the potentials which give reasonable description of the measured $\Lambda\Lambda$ correlation data, we discuss the corresponding potentials and resultant wave functions.

Since effects of interaction on the correlation function are incorporated through the difference from the free wave function as seen in Eq. (9), we display the integrand of the last term of Eq. (11) rather than the wave function itself in the right panel of Fig. 5 as well as the potentials in the left panel. The horizontal axis in the right panel is normalized by the size parameter R at the minimum χ^2 to reduce the apparent effect due to the different size in the source function. Although the wave function $\chi_Q(r)$ reflects the remarkable

TABLE III. $\Lambda\Lambda$ potential parameters with various effective ranges for fixed scattering length, $a_0 = -0.8$ fm, in the two-range Gaussian (TRG) form (2).

Model	$r_{\rm eff}$ (fm)	μ_1 (fm)	V_1 (MeV)	μ_2 (fm)	V_2 (MeV)
TRG02	2.0	0.6	−405.97	0.45	582.29
TRG04	4.0	0.6	−1835.95	0.45	4976.17
TRG06	6.0	0.6	−5569.58	0.45	25435.95
TRG08	8.0	0.8	−889.42	0.45	14595.38
TRG10	10.0	0.8	−1440.02	0.45	43254.42
TRG12	12.0	1.0	−358.38	0.45	20522.96

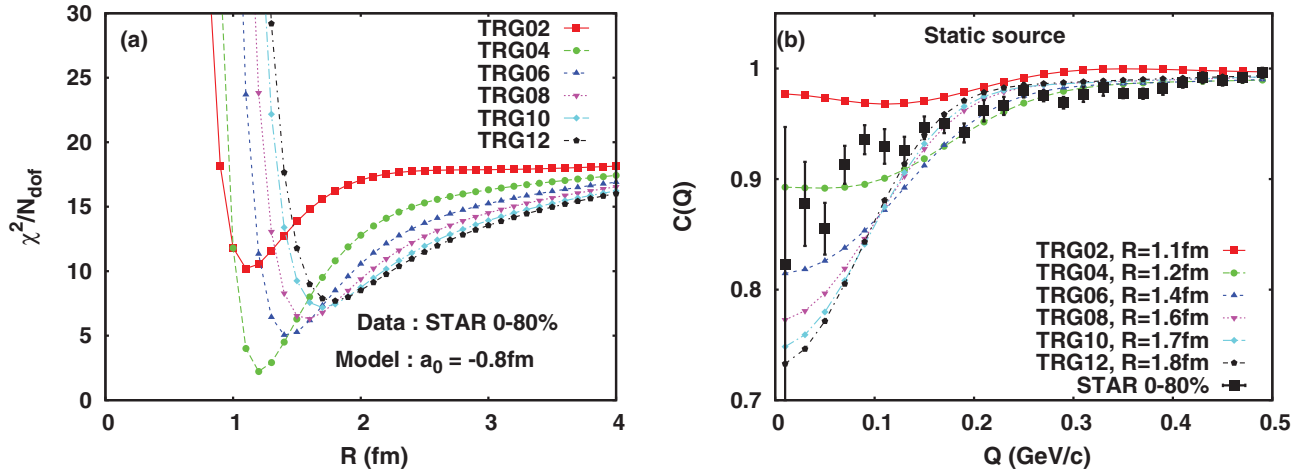

FIG. 4. (Color online) Results for TRG potentials. (a) $\chi^2/N_{\rm dof}$ against R. (b) $C(Q)$ at the minimum χ^2.

differences of the potentials at small r, $r^2e^{-r^2/4R^2}$ acts as a weight factor such that the behavior of the correlation function is most sensitive to the wave function at $r \simeq 1$–3 fm. One sees that the deviation from the free wave function is fairly reflected onto $C(Q)$. Namely, ND56 and NSC89-820, which show the largest attraction in the wave function at $r/R \simeq 1.5$, exhibit the strongest bunching in $C(Q)$, as seen in Fig. 3. ESC08, NF50, and fss2 also follow this trend. HKMYY, one of the two wave functions motivated by the Nagara event, has the weakest attraction among the potentials thus leads to the smallest deviation from $C(Q=0) = 0.5$ in Fig. 3. The other one, FG, has a somewhat stronger attraction, but the strongest repulsion around the origin leads to $\chi^2_Q < \chi^2_{\rm free}$ at $r < 0.5$ fm, which finally gives $C(Q) \simeq 0.8$ (see Fig. 3). It is instructive to note that fss2 and NF50 give a similar wave function despite the difference between the potentials. As given in Table I, both effective range and scattering length have close values in these potentials. This indicates that the $C(Q)$ is essentially determined by a_0 and $r_{\rm eff}$ rather than the detailed form of the potential.

The above consideration demonstrates how sensitive the correlation function $C(Q)$ is to the relative wave function. From the analysis with the static spherically symmetric source, strong constraints on the effective range and the scattering length of ΛΛ interaction have been obtained. The next step is to examine whether this capability is affected by the dynamics of relativistic heavy-ion collisions at the RHIC energy.

IV. EFFECT OF COLLECTIVITY

In the following, we consider source functions incorporating effects of expansion dynamics of the relativistic heavy-ion collisions. We assume that Λ particles are produced at the chemical freeze-out following the hadronization from quark-gluon plasma. Although Λ may interact with other produced hadrons and substantial amount of Λ multiplicity comes from decay of heavier particles, we assume that the information on ΛΛ interaction encoded in the correlation function is not distorted much by those hadronic effects. This simplification may be justified in part by the smaller Λ interaction with

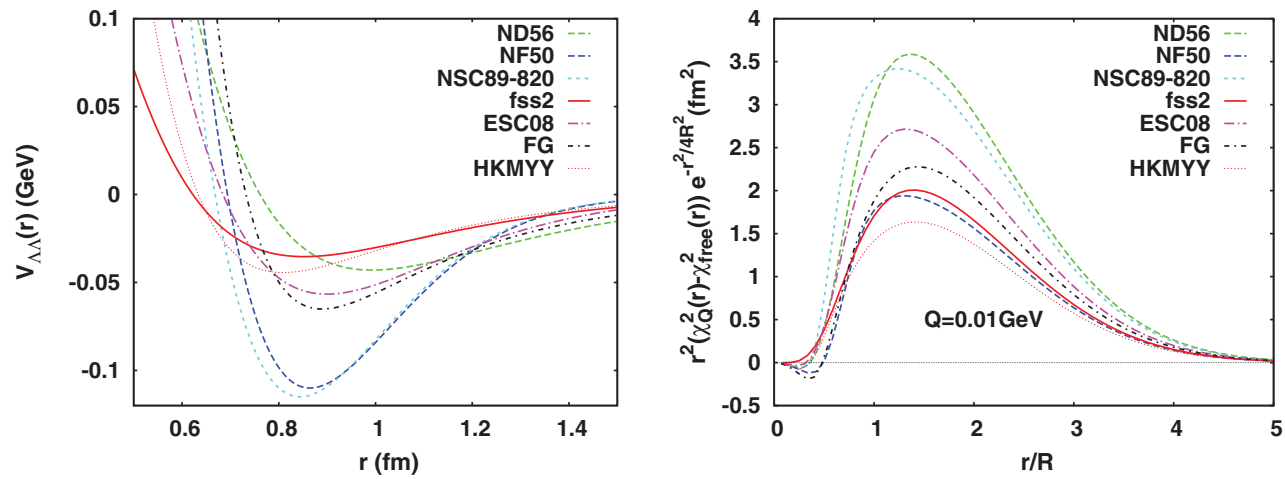

FIG. 5. (Color online) Left: ΛΛ potential for the selected parameter sets which fit the measured data well. Right: Deviation of the relative wave functions from the free one weighted with the source function at $Q = 0.01$ GeV.

the pion dominant environment and smaller feed-down effects expected in $\Lambda\Lambda$ correlation. Especially, if most of the weak and electromagnetic decay to Λ is removed by using the vertex detector, feed-down effects on Λ are expected to be small. We examine the feed-down effects in the next section and concentrate on the effects of collectivity in this section.

A. Models

Effects of the collective flow can be studied by modifying the source function $S(x,\boldsymbol{k})$. We utilize a thermal source model to implement the collective effect and change the source geometry to more relevant one for relativistic heavy-ion collisions. The collective flow velocity at the emission point x is denoted by u^μ and the Fermi distribution function $n_F(E,T) = (e^{E/T}+1)^{-1}$ for Λ is introduced to accommodate the thermal distribution in the rest frame of the emission point.

The source function is generally defined through the invariant spectrum

$$E\frac{d^3N}{d\boldsymbol{k}^3} = \int d^4x S(x,\boldsymbol{k}). \tag{13}$$

We consider several source functions to discriminate effects on the correlation function. As the simplest extension from the static source model used in the previous section, we implement the collective flow as

$$S_{\rm sph}(x,\boldsymbol{k}) = *u\cdot k\, n_F(u\cdot k,T) \times \exp\left[-\frac{x^2+y^2+z^2}{2R^2}\right]\delta(t-t_0). \tag{14}$$

The spherically symmetric flow velocity, $u^\mu = \gamma(1,\boldsymbol{v})$ where $\gamma = (1-v^2)^{-1/2}$, is assumed to exhibit a Hubble-type expansion $v = \tanh(\eta_r r/R)$. The coefficient η_r controls the strength of the expansion. The four momentum k is defined as on-shell one, $k^\mu = (E_k,\boldsymbol{k})$. The inner product $u\cdot k$ brings the space-momentum correlation into the source function if $\boldsymbol{v}\neq 0$. When $\eta_r = 0$, the space-momentum correlation of the source function is lost, i.e., the source function is factorized into $S(x,\boldsymbol{k}) = A(x)B(\boldsymbol{k})$ then the resultant correlation function reduces to that of the static source (11) because the momentum dependent part $B(\boldsymbol{k})$ is canceled by the denominator in Eq. (4).

While the above model (14) is useful to understand effects of the collective flow, the geometric part of the source function still possesses the spherical symmetry which is not appropriate for heavy-ion collisions at the RHIC energy. Owing to the huge colliding energy, the system undergoes rapid expansion along the collision axis (we take it as the z axis) followed by a slower one in the perpendicular direction. Therefore, we consider a cylindrically symmetric expanding system with the longitudinal boost invariance. The boost invariance also implies the infinite extent of the source in the collision axis. In the presence of the strong longitudinal flow, however, this does not mean that the source function has infinite width in the longitudinal direction since the thermal factor naturally gives a finite extent. In the Boltzmann approximation, one can derive an approximate but analytic expression for the longitudinal source size, $R_L \simeq \tau_0\sqrt{T/m_T}$ [32], where τ_0 denotes the freeze-out proper time and m_T is the transverse mass $m_T = \sqrt{p_x^2+p_y^2+m^2}$. The boost invariant approximation is of course valid only around the midrapidity region. At the RHIC energy, effects of possible deviation were found to be small [33].

In reality, collisions have finite impact parameters even in the highest multiplicity bin and event-by-event fluctuations may induce further asymmetry to the source. Those effects may be important for understanding experimental data on the $\pi\pi$ HBT correlation, but we shall ignore them since we are not aiming at extracting the source geometry but examining the final state interaction between Λ. The present statistics does not seem enough to project the $\Lambda\Lambda$ correlation function onto each direction of $\boldsymbol{Q}$. Thus, we assume the azimuthally symmetric Gaussian source profile. We expect this only leads to a smaller effective source size resulting from averaging over the azimuthal angle. In this case, we can put the average momentum $\boldsymbol{K}$ as $\boldsymbol{K} = (K_T,0,K_z)$ without loss of generality. Then a convenient source function has been used for the analysis of pion HBT radii in Ref. [34],

$$S_{\rm cyl}(x,\boldsymbol{k}) = \frac{m_T\cosh(y-Y_L)}{(2\pi)^3\sqrt{2\pi(\Delta\tau)^2}} n_f(u\cdot k,T) \times \exp\left[-\frac{(\tau-\tau_0)}{2(\Delta\tau)^2} - \frac{x^2+y^2}{2R^2}\right], \tag{15}$$

where $y = 1/2\ln[(E_k+k_z)/(E_k-k_z)]$ is the rapidity of the emitted particle. The Gaussian form of temporal part of the source function in the proper time $\tau = \sqrt{t^2-z^2}$ takes into account possible emission duration $\Delta\tau$ around a freeze-out time τ_0.

The four flow velocity can be parametrized by the longitudinal and transverse rapidity

$$u^t = \cosh Y_T \cosh Y_L, \tag{16}$$

$$u^z = \cosh Y_T \sinh Y_L, \tag{17}$$

$$u^x = \sinh Y_T \cos\phi, \tag{18}$$

$$u^y = \sinh Y_T \sin\phi. \tag{19}$$

The longitudinal flow rapidity is given by the scaling solution [35]

$$Y_L = \eta_s = \frac{1}{2}\ln\frac{t+z}{t-z}. \tag{20}$$

The transverse flow rapidity is assumed to be

$$Y_T = \eta_f\frac{r_T}{R}, \tag{21}$$

where $r_T = \sqrt{x^2+y^2}$ and η_f controls the strength of the transverse flow.

We fix the transverse flow strength parameter η_f from the single Λ spectra in Au+Au collisions at $\sqrt{s_{NN}} = 200$ GeV measured by the STAR Collaboration [36]. We use the 20–40% data since the detailed spectrum after feed-down subtraction is given. As we have ignored the baryon and the strangeness chemical potentials in the thermal description, we average the Λ and $\bar{\Lambda}$ data for the fit. Fixing $T = 160$ MeV, for the chemical freeze-out, we obtain that the minimum of $\chi^2/N_{\rm dof}$ is about 1.9 for $\eta_f = 0.33$. We use this value in the calculations

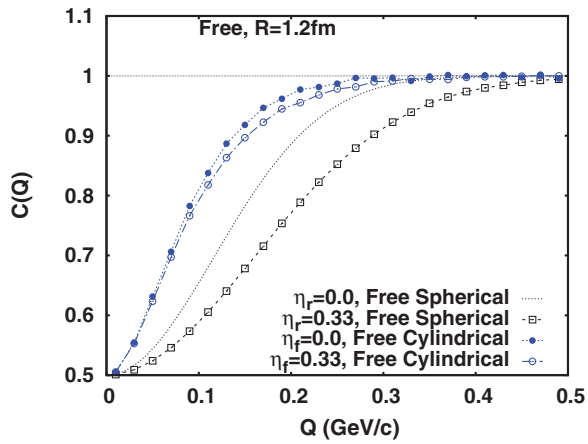

FIG. 6. (Color online) Free correlation functions for the spherically symmetric source (14) and for the cylindrically symmetric boost-invariant source (15). Closed and open symbols stand for $C(Q)$ with and without flow, respectively.

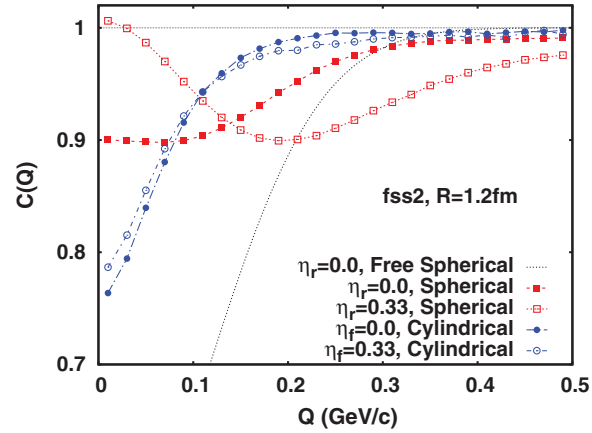

FIG. 7. (Color online) Correlation functions with fss2 interaction. Symbols are similar to the previous Fig. 6.

below.[1] Note that this can be determined independent of the size parameters, R, τ_0, and $\Delta\tau$. These parameters are regarded as free parameters to study the influence of the source geometry on the ΛΛ correlation function. Relations to the HBT radii have been extensively studied in Refs. [34] and [37] in the context of the π-π correlation.

B. Effects of collectivity

Now we calculate the ΛΛ correlation function for the expanding sources. Owing the space-time correlation induced by the collective flow, the correlation function depends on the average momentum $\boldsymbol{K}$ in addition to the relative one. We integrate the numerator and the denominator of Eq. (4) as

$$C(Q) = \frac{\int d^3\boldsymbol{K}\, W_2(\boldsymbol{k_1},\boldsymbol{k_2})}{\int d^3\boldsymbol{K}\, W_1(\boldsymbol{k_1}) W_1(\boldsymbol{k_2})}. \tag{22}$$

For the cylindrical source (15), the integration is carried out for the rapidity and the transverse momentum within the experimental acceptance ranges. For the spherical source, integration with respect to $|\boldsymbol{K}|$ is done for the same range as the transverse momentum in the cylindrical case, for simplicity. Although the following results may change quantitatively due to the average momentum dependence of the correlation function, these integrations do not lead to any change in our discussion below.

We begin with examining effects of collective flow in the spherically symmetric source to make a clear connection with the analyses in the previous section. We choose $R = 1.2$ fm in the model source function (14). Although not fitted to the experimental data, we apply the result of the fit to the p_T spectrum in the cylindrical source model and put $\eta_r = 0.33$. Figure 6 illustrates the effect of the flow strength on the free correlation functions. The dotted line stands for the static case $1 - \frac{1}{2}e^{-Q^2R^2}$. The expanding case is represented by open squares. One sees that the flow makes the correlation extended in the higher momentum region. In other words, the effective source size becomes smaller, as is well known for pion HBT radii [38,39]. In Fig. 7, we turn on the interaction between Λ by taking the fss2 potential. Since the difference of the potentials results in the relative wave function, our discussion in this section does not depend on the choice of the potential. By comparing with the $\eta_r = 0$ case, which is the same as fss2 result in Fig. 3, one finds that the correlation function resembles the more attractive potential. Since the interaction is not altered, one can understand this behavior as the effect of the collective flow. As shown in Fig. 6, effective source size is decreased by the collective flow. This can be understood as the result of position-dependent suppression of emission probability by the thermal factor [37]. This makes Λ pairs with small Q concentrated inside a small region thus they become more sensitive to the short range interaction.

Results for the cylindrical source function $S_{\rm cyl}$ (15) are also displayed in Figs. 6 and 7. Here we put $\tau_0 = 5$ fm and $\Delta\tau = 2$ fm. The free case with $\eta_f = 0$ is shown as closed circles in Fig. 6. The narrower width of the correlation function than that of the spherical source is due to the fact that η_f controls the transverse flow only and that the boost-invariant longitudinal expansion takes place. As seen in Eq. (15), the boost-invariant source function has infinite extent in the longitudinal direction if one ignores the thermal distribution. Although the longitudinal boost invariant expansion makes the effective source size finite, the source function has still a large longitudinal extent such that the behavior of $C(Q)$ resembles a larger source size than the spherically symmetric source. Since the longitudinal flow effect is dominant, the effect of the transverse flow seen through η_f is small. Note, however, that the effective source size becomes smaller by increasing η_f, because the same discussion as the case of the spherical source applies to the present result. As a result, the whole shape of the $C(Q)$ does not change much by the interaction. Nevertheless, the behavior of $C(Q)$ at low Q remains sensitive to the interaction, as depicted in Fig. 7. If we introduce a finite longitudinal size

[1] We checked that the choice of the temperature and the resultant flow strength do not influence our main objective in this paper, by repeating the same calculations for $T = 200$ MeV and 120 MeV.

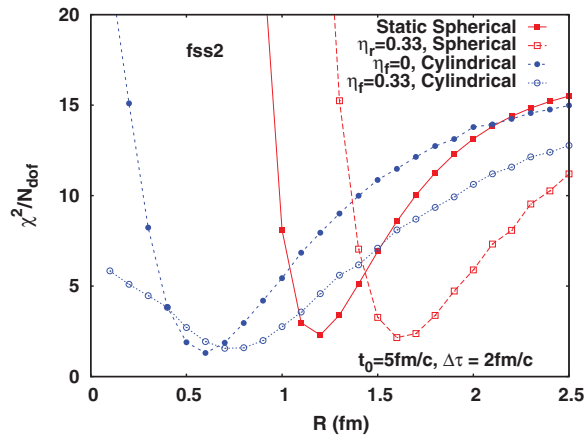

FIG. 8. (Color online) $\chi^2/N_{\rm dof}$ against the size parameter for the fss2 interaction.

into the source function, such as $e^{-z^2/2R^2}$, the behavior of the correlation function becomes closer to the case of the spherical source since the effective source size is reduced. We note that increasing τ_0 as well as $\Delta\tau$ also makes the effective source size larger, since τ_0 corresponds to the source extent in the z direction and $\Delta\tau$ contributes to the correlation function through the emission time difference in Eq. (4).

As a result of geometry and flow effects, the optimal source size is modified from that in the spherical static source case. In Fig. 8, we show the size parameter dependence of $\chi^2/N_{\rm dof}$ with the fss2 interaction. For the spherical geometry, the optimal source size is shifted to the larger direction by 30–40%. Figure 9 shows the corresponding correlation functions at the minimum of χ^2. Interestingly, despite the difference in the source size, the resultant correlation functions for $\eta_r = 0$ and 0.33 with the spherical source are almost the same. The effect of the flow is absorbed into the larger optimal source size.

For the cylindrical and boost invariant source, the optimal transverse source size is also shifted upwards, while the shift is smaller as discussed above. The behavior of the χ^2 in small R reflects the effect of the geometry and the flow. Since the

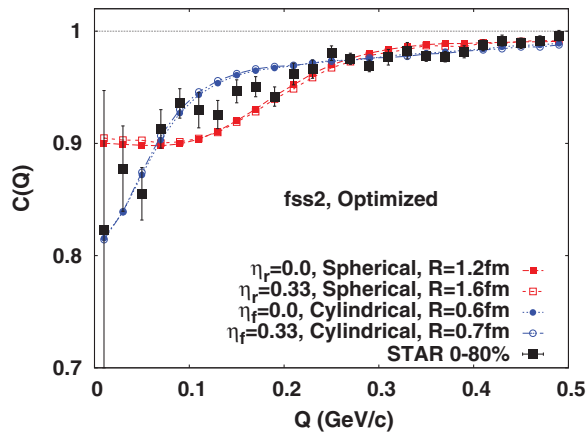

FIG. 9. (Color online) $\Lambda\Lambda$ correlation function with fss2 interaction for the spherical and the cylindrical boost-invariant source optimized for minimum χ^2.

source function is elongated in the longitudinal direction, the source has a longitudinal extent even when R is so small. Thus Λ particles feel less attraction than in the case of the spherical source with small R. The transverse flow further reduces the variation of $C(Q)$ against R. It is interesting to note that despite almost the same value of $\chi^2/N_{\rm dof}$ of the cylindrical source as that of the spherical source, the optimized correlation function shown in Fig. 9 has a different feature. The result of the cylindrical source indicates that $C(Q)$ with the small width also describes the data well if this shape of $C(Q)$ can be obtained, though it was not possible in the spherical source as shown in Sec. III.

Then, we have performed the same analysis for other $\Lambda\Lambda$ interactions. We found that the favored $\Lambda\Lambda$ interactions are the same as those in the case of the spherical static source $S_{\rm stat}$. However, we also found that interactions with larger effective range and smaller scattering length are favored. For example, among ND interactions, ND58 is now better than ND56, contrary to the case of $S_{\rm stat}$ (Fig. 2), while ND56 still gives a good fit, too. NSC97 potentials are also found to be improved, but $\chi^2/N_{\rm dof} \simeq 8$ at the best in NSC97c and NSC97e. NSC97d no longer shows a good fit with the cylindrical source model $S_{\rm cyl}$. This indicates that the good fit in $S_{\rm stat}$ (Fig. 2) was a spurious one, not due to the interaction but to an accidental geometric effect.

χ^2 and the optimized $C(Q)$ for all the potential that give $\chi^2/N_{\rm dof} < 8$ are summarized in Fig. 10. Since ND58 and FG have almost the same a_0 and $r_{\rm eff}$, the result is so. Other $\Lambda\Lambda$ interactions give larger χ^2. In Fig. 1, we mark the favored $\Lambda\Lambda$ interaction with big circles. The scattering parameters of these interactions are in the range $-1.8\ {\rm fm}^{-1} < 1/a_0 < -0.8\ {\rm fm}^{-1}$ and $3.5\ {\rm fm} < r_{\rm eff} < 7\ {\rm fm}$. Potentials studied in this work and outside of this region give larger χ^2, $\chi^2/N_{\rm dof} > 5$, at any value of the source size and with any geometry and flow values. One sees that the small size is favored owing to somewhat scattered data points and larger errors in the small Q region. The difference of the correlation function in those potentials is of the same size as experimental errors for $0.1 < Q < 0.2$ GeV and even larger at $Q < 0.1$ GeV. Therefore, the data give a strong constraint on the interaction potential of the $\Lambda\Lambda$ system. Indeed, the favored potentials obtained from this analysis agrees well with the results obtained in the analysis of $^{12}{\rm C}(K^-, K^+)$ $\Lambda\Lambda X$ reaction [9]. Enhancement of the $\Lambda\Lambda$ invariant mass spectrum at low energies are well described by the final state interaction effects with fss2 [25] and ESC04d [40]. The scattering length and the effective range in ESC04d interaction are $a_0 = -1.323$ fm and $r_{\rm eff} = 4.401$ fm, respectively, which are inside the region obtained in the present analysis. The analyses of $\Delta B_{\Lambda\Lambda}$ in the Nagara event [2,3] show $\Lambda\Lambda$ interactions which are inside the allowed region.

V. FEED-DOWN CONTRIBUTION

A. Estimate of feed-down contribution

So far we have assumed that Λ baryons are directly emitted from the hot matter. This assumption would be valid if one could remove the decay contribution from parent particles such as Ξ and Σ^0 or the correlation function $C(Q)$ was not

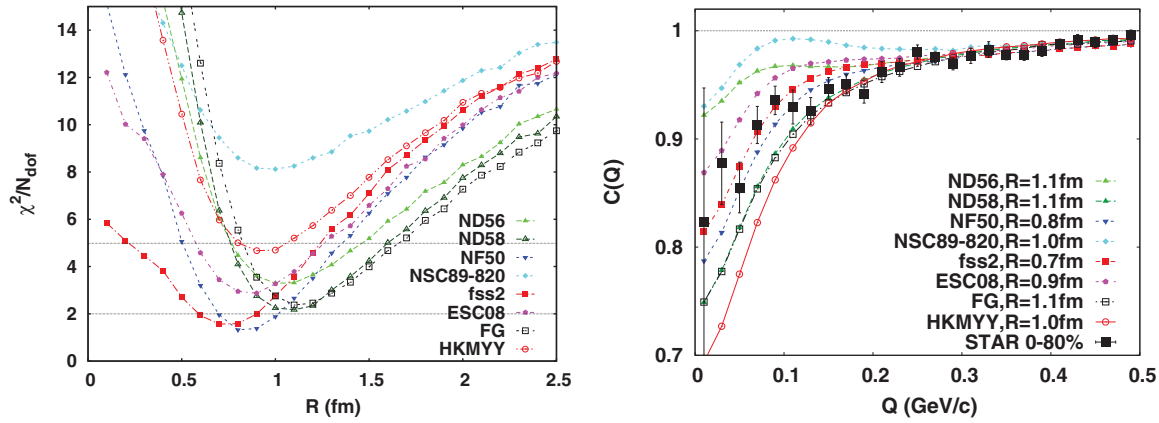

FIG. 10. (Color online) Left: $\chi^2/N_{\rm dof}$ for the favored potentials in the cylindrical source model with collective flow (15). Right: corresponding ΛΛ correlation functions at the minimum χ^2.

affected by such a feed-down contribution. In the case of the $\pi\pi$ correlation function, it has been known that long-lived parents give a sharp correlation near $Q \simeq 0$ which cannot be resolved and thus cause an apparent reduction of the intercept $C(Q=0)$ [41–43]. The same argument applies to the ΛΛ correlation as well. For $N_{\rm tot}$ being the total number of measured Λ and N^p being the long-lived parents decaying into Λ, respectively, the effective intercept λ is given by

$$\lambda = \left(1 - \frac{N^p}{N_{\rm tot}}\right)^2. \tag{23}$$

The correlation function after the feed-down correction to the bare one reads

$$C_{\rm corr}(Q) = 1 + \lambda[C_{\rm bare}(Q) - 1], \tag{24}$$

which should be confronted with the data.

The contribution to $N_{\rm tot}$ mainly consists of Σ(1385), Σ^0, Ξ, as well as direct Λ and heavier resonances such as Ω are negligible. Since decay width of Σ(1385) is 36–40 MeV, this contribution will give the Λ source function an effectively long lifetime and might influence low Q behavior of $C(Q)$, but will not affect λ. Thus, we do not treat daughters from Σ(1385) as a part of the long-lived parents but regard them as a part of direct Λ. One needs to invoke dynamical simulations for more serious estimates of these short-lived resonance effects.

Then N^p consists of the contribution from Σ^0 and Ξ. The fraction of Σ^0 to Λ in heavy-ion collisions is not experimentally known, because of the difficulty in reconstruction of the $\Sigma^0 \to \Lambda\gamma$ process. Here we utilize an experimental result in p + Be collisions at $p_{\rm lab} = 28.5$ GeV [44], $N_{\Sigma^0}/N_\Lambda = 0.278$. Although the production process of the hyperons in pA collisions could be different from that in heavy-ion collisions, we note that this ratio is consistent with thermal model calculations [45].

Ξ yields in Au+Au collisions at $\sqrt{s_{NN}} = 200$ GeV has been shown to 15% of total Λ [36]. Here we assume that a part of the Ξ decay contribution to Λ is excluded by the candidate selection employed in the STAR measurement [15], according to the distance of closest approach less than 0.4 cm which is comparable to minimum decay length of Ξ. Combining these fractions of resonances to Λ and subtracting the Ξ contributions from $N_{\rm tot}$, We obtain $\lambda = (0.67)^2$. If we take account of the Ξ contribution into the total yields, $\lambda = (0.572)^2$. Since the above selection does not exclude all of Ξ, the realistic value could be a little smaller than $(0.67)^2$, but larger than $(0.572)^2$. We estimate the higher resonance contribution to $N_{\rm tot}$ to within a few percent. Therefore, we reanalyze the data by correcting

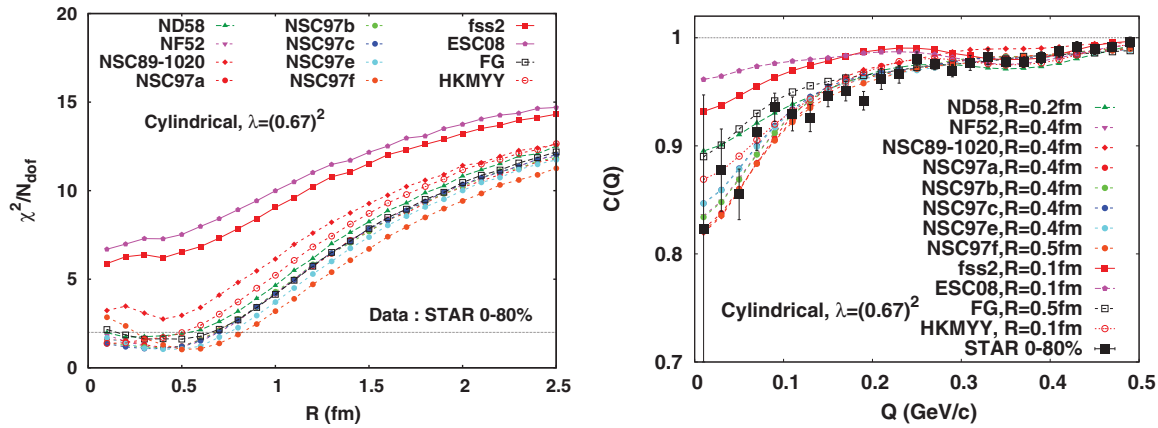

FIG. 11. (Color online) Same as Fig. 10, but corrected for Σ^0 feed-down contribution by $\lambda = (0.67)^2$.

the correlation function obtained from the cylindrical source function (15), with $\lambda = (0.67)^2$. We confirmed that the lower value $\lambda = (0.572)^2$ only gives quantitative change in $\chi^2/N_{\rm dof}$ values in the following analyses.

B. Effects on correlation function

Results of reanalysis with the feed-down contribution are shown in Fig. 11. The correction factor $\lambda = (0.67)^2$ leads to $C(Q = 0) = 0.776$. This implies the reduction of not only the intercept, but also the whole correlation function. As a result, $C(Q)$ becomes less sensitive to the difference among the potentials and we have more potentials which can fit the data. For instance, NSC97 potentials now reproduce the data except for NSC97d. However, one immediately notes that the potentials reproduce the data with unphysically small transverse size, $R \leqslant 0.5$ fm. Owing to the multiplicative factor λ, the tail of $C(Q)$ becomes closer to unity. Then the smaller size is preferred to fit the long tail in the STAR data. Thus if we adopt the smaller value of λ, the minimum of χ^2 shifts to smaller R values. As explained in Sec. IV, the smaller size is accompanied by the stronger effect of the attraction. ND56 and NSC89-820, which already overshoot the data in the uncorrected case due to too strong attraction in Fig. 10, can no longer reproduce the data while some of those with weaker attraction fit the data well. fss2 and ESC08 overshoot the data despite the weaker attaction. Nonmonotonic behavior in $\chi^2/N_{\rm dof}$ indicate that both may fit the low Q region with $R \simeq 0.4$ fm, but minimum χ^2 cannot be achieved due to the tail of $C(Q)$.

C. Residual correlation

The agreement between the data and models at the small source size cannot be a physically reasonable result. It rather suggests that there exist additional sources of the correlation which give the long tail of $C(Q)$. In Ref. [15], a Gaussian term with two additional fitting parameters $a_{\rm res}$ and $r_{\rm res}$,

$$C_{\rm res}(Q) = a_{\rm res} e^{-r_{\rm res}^2 Q^2}, \tag{25}$$

is employed in the fitting function $C_{\rm fit}(Q)$ to account for the long tail as a residual correlation, presumably caused by parent particles. While this prescription is found to improve the quality of the fit, the origin is not known. Here we investigate effects of the additional term by evaluating χ^2 as a function of $a_{\rm res}$ and $r_{\rm res}$ for each of source size R.

Figure 12 shows results including the residual correlation term for potentials which give reasonable fits to the data before the feed-down correction. One sees that $\chi^2/N_{\rm dof} \simeq 1$ independent of the size parameter for $R > 0.5$ fm. The strength $a_{\rm res}$ and the spatial size parameter $r_{\rm res}$ of the residual correlation exhibit R dependence. In particular, for $R < 1$ fm, $r_{\rm res}$ becomes larger as R is decreased and eventually $r_{\rm res} > R$. On the other hand, $r_{\rm res}$ and $a_{\rm res}$ for different potentials approach to common values as R increases. These tendencies might indicate a two-source structure in the data. Although unrealistic, in the case of small R and large $r_{\rm res}$, the large variation in the strength $a_{\rm res}$ (see the middle panel of Fig. 12) indicates that the low Q behavior is dominated by the residual term and the long tail of $C(Q)$ is fitted with the interaction and the collective effects in

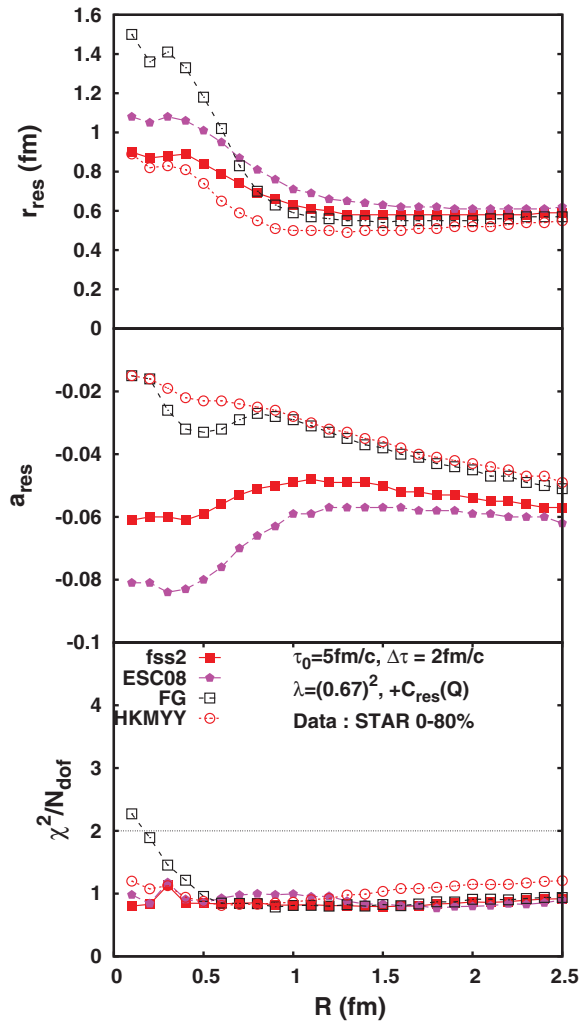

FIG. 12. (Color online) Residual correlation parameters as functions of R for fss2, ESC08, FG, and HKMYY potentials. Bottom: minimum of χ^2. Top and middle panels: $r_{\rm res}$ and $a_{\rm res}$ giving the minimum χ^2, respectively.

the source function by small R. In this case, the role of each term is inverted but the general structure is kept such that the low Q part is sensitive to the interaction and the high Q tail is attributed to a correlation in a small size. The two source structure might be more natural for small $r_{\rm res}$ and large R, in which $r_{\rm res}$ approaches to 0.6 fm and R is comparable to source sizes extracted from proton-proton correlation measurements.

We find that the same behavior is also seen in other potentials with $1/a_0 \leqslant -0.8$ fm. The feed-down correction reduces the sensitivity to $\Lambda\Lambda$ interaction in the low Q region. Consequently, the data no longer constrains the effective range, as demonstrated in Fig. 13, where the correlation functions are plotted for $R = 2.5$ fm, in accordance with the χ^2 analysis in Fig. 12. All the shown potentials fit the data well and no difference is seen in $Q > 0.15$ GeV/c. At low Q, albeit small, $C(Q)$ exhibits interaction dependence fairly reflecting the strength of attraction, similarly to the right panel of Fig. 10. Note, however, that FG and fss2 have a factor of 2 different effective range while they have almost the same

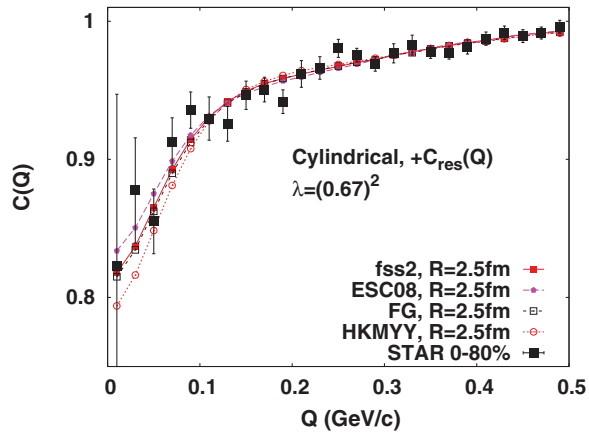

FIG. 13. (Color online) Correlation functions combined with the residual term and the feed-down correction for $R = 2.5$ fm.

scattering length. We also find that all the NSC97 potentials, of which $r_{\rm eff}$ is broadly ranged from 1.15 to 16.33 fm and the scattering length is $1/a_0 < -2$ fm^{-1}, can reproduce the data with $\chi^2/N_{\rm dof} \simeq 1$.

In general, results with the residual correlation term (25) depends on the feed-down contribution λ. Since the value $\lambda = (0.67)^2$ takes only Σ^0 into account, this serves a minimal correction owing to possible Ξ contribution. We confirmed that the present result for the constraint on the scattering length, $1/a_0 < -0.8$ fm, holds for smaller λ by repeating the same analyses for $\lambda = (0.572)^2$ in which the Ξ contribution is included.

The above discussion applies to all the potentials with $a_0 < 0$ analyzed here. We note that there are two exceptions. We find that ND46 and NF42, which have the positive largest $1/a_0$ thus have a bound state, can fit the data when $R < 0.7$ fm with the residual correlation taking $2 < r_{\rm res} < 4$ fm and $-0.2 < a_{\rm res} < -0.08$. We consider it to be coincidence, since it is accompanied with $r_{\rm res}$ larger than the source size and $\chi^2/N_{\rm dof} \sim 1$ is achieved only in the small R region. As we shall discuss below, the appearance of the bound state should lead to suppression of $C(Q)$ at low Q when the source size is larger than a_0. Therefore, one may be able to confirm or rule out this possibility by analyzing data of more central collisions, which are expected to have a larger source size.

VI. DISCUSSION

A. Possible signal of H resonance

On the basis of the scattering length and the effective range of the $\Lambda\Lambda$ interaction obtained in the present analyses, the existence of the H particle as a bound state of $\Lambda\Lambda$ is not preferred. This can be understood from the enhanced $\Lambda\Lambda$ correlation function observed in the data compared with the free case. If we had a bound state in $\Lambda\Lambda$, the correlation function would be suppressed from the free case. The scattering wave function has the asymptotic form, $\chi_q(r) = e^{-i\delta}\sin(qr+\delta)/qr$, where $q = Q/2$ is the relative momentum of Λ. In the case of small enough interaction range compared with the source size, we can substitute the asymptotic form for the scattering wave function $\chi_q(r)$ in Eq. (11) and obtain the low energy limit of the correlation function,

$$C(Q) \to \frac{1}{2} - \frac{1}{\sqrt{\pi}}\frac{a_0}{R} + \frac{1}{4}\left(\frac{a_0}{R}\right)^2 \quad (Q \to 0), \qquad (26)$$

where the phase shift is given approximately as $\delta \simeq -a_0 q$. For $\Lambda\Lambda$ interaction with a bound state ($a_0 > 0$), the scattering wave function has a node at $r \simeq a_0$ at low energies, then the correlation function is suppressed compared with the free case in the low energy limit, as long as the second term dominates in Eq. (26). Thus we would see a suppressed Q region if we have a bound state. In practice, the interaction range is not small enough compared with the source size considered here, thus the above estimate might not be precise. It should be noted that the above argument is not valid, when $\Lambda\Lambda$ is not the dominant component of H.

The existence of H as a resonance pole above the $\Lambda\Lambda$ threshold is another interesting possibility, as suggested in KEK experiments [8,9]. While the $\Lambda\Lambda$ potentials considered here do not have H as an s-wave resonance, a quark model calculation with instanton induced interaction allows the existence of resonance H below the ΞN threshold [46]. In order to evaluate the strength of the resonance H signal in the correlation function, we have invoked the statistical model results. In the statistical model [47], H (Λ) yield is calculated to be $N_H \simeq 1.3 \times 10^{-2}$ ($N_\Lambda \simeq 30$) per event per unit rapidity. We here assume that the resonance H is produced in a different mechanism from the $\Lambda\Lambda$ potential scattering. We also assume that the mass of H is distributed according to the Breit-Wigner function, then the contribution of resonance H in the $\Lambda\Lambda$ relative momentum spectrum is given as

$$\frac{dN_H}{dydQ} = N_H f_{\rm BW}(E_Q)\frac{dE_Q}{dQ}, \qquad (27)$$

where $f_{\rm BW}(E) = \Gamma_H/[(E-E_H)^2 + \Gamma_H^2/4]/2\pi$ is the Breit-Wigner function. In Fig. 14, we show the strength of the resonance H signal. We have fitted the STAR data in a simple smooth function, and added the ratio of $dN_H/dydQ$ to the thermal $\Lambda\Lambda$ distribution, $dN_{\Lambda\Lambda}/dydQ = 4\pi q^2 N_{\Lambda\Lambda}\exp(-q^2/2\mu T)/(2\pi\mu T)^{3/2}/2$, where $q = Q/2$,

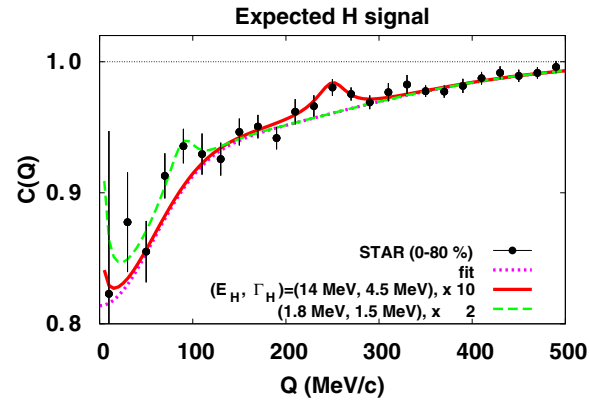

FIG. 14. (Color online) Possible resonance H signal in the $\Lambda\Lambda$ correlation function. Signal for $(E_H,\Gamma_H) = (14$ MeV, 4.5 MeV) and $(E_H,\Gamma_H) = (1.8$ MeV, 1.5 MeV) are multiplied by 10 and 2, respectively.

$N_{\Lambda\Lambda} = N_\Lambda^2$ and $\mu = M_\Lambda/2$. The signal enhanced by a multiplication factor. The resonance parameters and the multiplication factor are chosen so as to fit the bump structure in the data as if the bump is the resonance H signal.

We find that the resonance H signal relative to the thermal background is small and higher statistics is necessary to confirm its existence, especially when the resonance energy is large, $E_H > 10$ MeV. In order to demonstrate this point, we show the results with $(E_H,\Gamma_H) = (14\ \text{MeV},4.5\ \text{MeV})$ and $(E_H,\Gamma_H) = (1.8\ \text{MeV},1.5\ \text{MeV})$, where the signal is multiplied by 10 and 2, respectively. In the case where the resonance energy is large, the signal is in the same order of the bump height after being multiplied by 10. The bump structure around 14 MeV ($Q \sim 250$ MeV/c) in the correlation function data for the 0–80% centrality seems to come from statistical fluctuations and is not considered to be the signal of the resonance H, since the position and height depend on the centrality [48]. If the resonance H exists at small energy above the $\Lambda\Lambda$ threshold, it may be possible to detect the signal. The bump in the data at around 1.8 MeV ($Q \sim 90$ MeV/c) is also considered to come from the statistical fluctuation, and its strength is about twice the statistical model estimate of the H signal. If we can reduce the error to half, it would be possible to confirm or rule out the existence of resonance H at low energies.

B. Implication to $\Lambda\Lambda$ N three-body interaction

Another interesting implication of the present analyses is the difference between the vacuum and in-medium $\Lambda\Lambda$ interactions. The $\Lambda\Lambda$ interactions in Refs. [2,3] may be less attractive than those expected from the $\Lambda\Lambda$ correlation data; as seen in Figs. 3 and 10, $\Lambda\Lambda$ correlations from these two interactions tend to be smaller than the data. The strengths of these $\Lambda\Lambda$ interactions are fitted to the $\Lambda\Lambda$ bond energy in the Nagara event $\Delta B_{\Lambda\Lambda} = 1.01 \pm 0.20^{+0.18}_{-0.11}$ MeV [1]. The $\Lambda\Lambda$ bond energy was recently updated to be a smaller value, $\Delta B_{\Lambda\Lambda} = 0.67 \pm 0.16$ MeV ($B_{\Lambda\Lambda} = 6.91$ MeV) [49] following the Ξ^- mass update by the Particle Data Group [50]. The updated $\Delta B_{\Lambda\Lambda}$ value could imply further weaker $\Lambda\Lambda$ interaction. For example, the HKMYY interaction was updated to fit the new $\Delta B_{\Lambda\Lambda}$ [51], and the scattering parameters become $(a_0,r_{\text{eff}}) = (-0.44\ \text{fm},10.1\ \text{fm})$,which is outside of the favored region based on the analyses without the feed-down correction.

While it is still premature to draw any conclusion, a less attractive $\Lambda\Lambda$ interaction in nuclei than the interaction in vacuum would suggest the density dependence of the $\Lambda\Lambda$ interaction. A part of $\Lambda\Lambda$ attraction comes from the coupling with the ΞN channel $\Lambda\Lambda \leftrightarrow \Xi N$, since the threshold energy difference is small, $M_\Xi + M_N - 2M_\Lambda \sim 28$ MeV. The Pauli blocking in the ΞN channel leads to reducing the attraction in the $\Lambda\Lambda$ channel. All the nucleon $0s$ states are occupied in ${}^{6}_{\Lambda\Lambda}$He, the nucleon in the intermediate state has to be in the p state, and the coupling effect is suppressed. Myint, Shinmura, and Akaishi found that the coupled channel Pauli suppression effect results in the reduction of the bond energy in ${}^{6}_{\Lambda\Lambda}$He by 0.09, 0.43, and 0.88 MeV for the ND, NSC97e, and NF coupling strength, respectively [52]. Their result with NSC97e interaction $\Delta B_{\Lambda\Lambda} = 0.64$ MeV roughly coincides with the updated value, but their estimate of the scattering parameters $(a_0,r_{\text{eff}}) = (-0.5\ \text{fm},8.41\ \text{fm})$ is outside the favored region by the STAR data in which the feed-down correction is not taken into account. It would be an interesting issue whether $\Lambda\Lambda$ interaction with strong coupling with the ΞN channel can consistently explain the Nagara event and the RHIC data.

The coupled channel Pauli suppression is found to be one of the important origins to generate repulsive contribution in nuclear matter at high density [53]. Thus further investigations of $\Lambda\Lambda$ correlation and double hypernuclei would open a way to access the density dependence of the $\Lambda\Lambda$ interaction, or the $\Lambda\Lambda$ N three-body interaction, which would be important to understand the origin of the additional repulsion required to support massive neutron stars with strange hadrons [5].

C. Comparison with the previous work

Before closing the section, we briefly comment on the analysis by the STAR Collaboration in [15]. Using the Lednický and Lyuboshitz analytical model, they found that the same data favor, albeit weak, a repulsive interaction $a_0 > 0$ in contrast to our analysis suggesting weakly attractive interaction; the phase shift at low energies, $\delta \simeq -a_0 k$, increases when $a_0 < 0$ as suggested in the present work, while it decreases when $a_0 > 0$ as in the analysis by the STAR Collaboration.[2]

The main reason for this discrepancy would come from the difference in the treatment of the intercept parameter λ. In the analysis in [15], it is a fitting parameter to obtain minimum χ^2 while we fix it from yields of parent particles decaying to λ. Their result $\lambda = 0.18 \pm 0.05^{+0.12}_{-0.06}$ is much smaller than ours, and gives $C(0)$ closer to unity. A small value of λ leads to a small bare correlation $C_{\text{bare}}(Q)$ at small Q as found from Eq. (24), and the low energy value would be less than the free value, $C_{\text{bare}}(Q \to 0) < 0.5$, implying a repulsive interaction. This indicates the importance to understand the λ value in the analysis of $\Lambda\Lambda$ correlation aiming at extracting the interactions.

VII. CONCLUDING REMARKS

We have studied the $\Lambda\Lambda$ correlation function in relativistic heavy-ion collisions. By using a simple static source model, we illustrate how the correlation function is sensitive to differences in interaction potentials. From fits to the measured experimental data, it turned out that the favored potentials have small negative scattering length and effective range around 4 fm. Then we examined effects of the collective expansion on the behavior of the correlation function by making use of a thermal source model with the boost-invariant expansion along the collision axis and transverse expansion fitted to the p_T spectrum. We point out that the strong expansion modifies the behavior of the correlation function at small Q, but it remains sensitive to the potential. In particular, it

[2]Note that the sign convention of a_0 is different from that in the present paper.

turns out that the same potentials as the static source case are favored. We have obtained a set of the potentials which give a reasonable fit to the data with a small transverse size, under an assumption that feed-down correction to the correlation function is negligible. Such potentials are characterized by the scattering length $-1.8\ \mathrm{fm}^{-1} < 1/a_0 < -0.8\ \mathrm{fm}^{-1}$ and the effective range $3.5\ \mathrm{fm} < r_{\mathrm{eff}} < 7\ \mathrm{fm}$, as represented by a thick shaded area in Fig. 1.

In the above analysis, we treat the size parameter R as a fitting parameter to the experimental data. The obtained source size is found to be somewhat smaller than the HBT radii for protons. Discussion on the collision dynamics based on the size, as done in pion HBT studies, is beyond our scope in this paper. A possible reason might be small scattering cross sections of Λ with other particles, which give the correlation function less sensitive to the later stage of the collision process. Although the agreement of the favored potentials between the static source model and the boost-invariant source model analyses seems to suggest irrelevance of the detailed dynamics of collisions, our findings should be confirmed by studies with more realistic source models.

We have also studied effects of feed-down correction from $\Sigma^0 \to \Lambda\gamma$ decay in analogy with effects of long-lived particles in the pion HBT. The reduction of the intercept parameter λ is found to reduce the sensitivity of the correlation function to ΛΛ interaction in low Q and lead to unphysically smaller source size to fit the high Q tail. To remedy this, we have considered an additional Gaussian term in the correlation function and found that the data is well described by the two source structure. We confirmed that the low Q part remains sensitive to the interaction with coarse resolution such that the correlation function is no longer sensitive to the effective range. The resultant constraint on the scattering length is found to be $1/a_0 < -0.8\ \mathrm{fm}^{-1}$. In this case, the source size is roughly consistent with proton HBT radii, but the long tail in Q is attributed to the additional term whose origin is not known.

Since this term can be attributed to a source with small size, it might suggest a different source of Λ production such as a two-step hadron production mechanism, in which inhomogeneous matter is first formed and decays into hadrons later.

Nevertheless, the agreement of the favored potentials in this work with the most recent ΛΛ potential models (fss2 and ESC08) indicates the relevance of our study and demonstrates the feasibility of using the ΛΛ correlation function to extract the interaction. Furthermore, channel coupling needs to be taken care of for a better understanding of data. Preliminary analysis [17] shows that the coupling with the ΞN channel is not significant as long as the coupling potential is not very strong. A more consistent treatment and data with higher statistics are desired to pin down the ΛΛ interaction.

ACKNOWLEDGMENTS

The authors would like to thank N. Shah and H. Z. Huang for providing them the STAR data. They also would like to acknowledge T. Rijken, S. Shinmura, Y. Yamamoto, E. Hiyama, A. Gal, Y. Akaishi, and B. Müller for helpful discussions. K.M. would like to thank K. Redlich for discussion on Σ^0 decay and hyperon yields in thermal models. He also acknowledges other members of Institute of Theoretical Physics in University of Wroclaw for discussion. Numerical computations were carried out on SR16000 at YITP in Kyoto University. This work was supported in part by the Grants-in-Aid for Scientific Research from JSPS [Grants No. (B) 23340067, No. (B) 24340054, No. (C) 24540271], by the Grants-in-Aid for Scientific Research on Innovative Areas from MEXT (Area No. 2404, Grants No. 24105001, No. 24105008), by the Yukawa International Program for Quark-Hadron Sciences, by HIC for FAIR, and by the Polish Science Foundation (NCN), under Maestro Grant No. 2013/10/A/ST2/00106.

[1] H. Takahashi *et al.*, Phys. Rev. Lett. **87**, 212502 (2001).
[2] I. N. Filikhin and A. Gal, Nucl. Phys. A **707**, 491 (2002).
[3] E. Hiyama, M. Kamimura, T. Motoba, T. Yamada, and Y. Yamamoto, Phys. Rev. C **66**, 024007 (2002).
[4] N. K. Glendenning, Astrophys. J. **293**, 470 (1985); Y. Sugahara and H. Toki, Prog. Theor. Phys. **92**, 803 (1994); J. Schaffner and I. N. Mishustin, Phys. Rev. C **53**, 1416 (1996); S. Balberg and A. Gal, Nucl. Phys. A **625**, 435 (1997); M. Baldo, G. F. Burgio, and H. J. Schulze, Phys. Rev. C **61**, 055801 (2000); I. Vidana, A. Polls, A. Ramos, M. Hjorth-Jensen, and V. G. J. Stoks, *ibid.* **61**, 025802 (2000); S. Nishizaki, T. Takatsuka, and Y. Yamamoto, Prog. Theor. Phys. **108**, 703 (2002); H. Shen, Phys. Rev. C **65**, 035802 (2002); C. Ishizuka, A. Ohnishi, K. Tsubakihara, K. Sumiyoshi, and S. Yamada, J. Phys. G **35**, 085201 (2008).
[5] P. Demorest, T. Pennucci, S. Ransom, M. Roberts, and J. Hessels, Nature (London) **467**, 1081 (2010).
[6] R. L. Jaffe, Phys. Rev. Lett. **38**, 195 (1977); **38**, 617 (1977).
[7] S. R. Beane *et al.* (NPLQCD Collaboration), Phys. Rev. Lett. **106**, 162001 (2011); T. Inoue, N. Ishii, S. Aoki, T. Doi, T. Hatsuda, Y. Ikeda, K. Murano, H. Nemura, and K. Sasaki (HAL QCD Collaboration), *ibid.* **106**, 162002 (2011).
[8] J. K. Ahn *et al.* (KEK-PS E224 Collaboration), Phys. Lett. B **444**, 267 (1998).
[9] C. J. Yoon, H. Akikawa, K. Aoki, Y. Fukao, H. Funahashi, M. Hayata, K. Imai, K. Miwa *et al.*, Phys. Rev. C **75**, 022201(R) (2007).
[10] Y. Nara, A. Ohnishi, T. Harada, and A. Engel, Nucl. Phys. A **614**, 433 (1997).
[11] R. Lednicky and V. L. Lyuboshits, Sov. J. Nucl. Phys. **35**, 770 (1982) [Yad. Fiz. **35**, 1316 (1981)]; M. Gmitro, J. Kvasil, R. Lednicky, and V. L. Lyuboshitz, Czech. J. Phys. B **36**, 1281 (1986); R. Lednicky, V. V. Lyuboshitz, and V. L. Lyuboshitz, Phys. Atom. Nucl. **66**, 975 (2003) [Yad. Fiz. **66**, 1007 (2003)]; R. Lednicky, Phys. Part. Nucl. **40**, 307 (2009).
[12] W. Bauer, C. K. Gelbke, and S. Pratt, Ann. Rev. Nucl. Part. Sci. **42**, 77 (1992).
[13] C. Greiner and B. Müller, Phys. Lett. B **219**, 199 (1989).
[14] A. Ohnishi, Y. Hirata, Y. Nara, S. Shinmura, and Y. Akaishi, Nucl. Phys. A **670**, 297 (2000).

[15] L. Adamczyk *et al.* (STAR Collaboration), Phys. Rev. Lett. **114**, 022301 (2015).
[16] N. Shah (for the STAR Collaboration), Acta Phys. Pol. Suppl. **5**, 593 (2012).
[17] A. Ohnishi *et al.* (ExHIC Collaboration), Nucl. Phys. A **914**, 377 (2013).
[18] M. M. Nagels, T. A. Rijken, and J. J. de Swart, Phys. Rev. D **15**, 2547 (1977).
[19] M. M. Nagels, T. A. Rijken, and J. J. de Swart, Phys. Rev. D **20**, 1633 (1979).
[20] P. M. M. Maessen, T. A. Rijken, and J. J. de Swart, Phys. Rev. C **40**, 2226 (1989).
[21] T. A. Rijken, V. G. J. Stoks, and Y. Yamamoto, Phys. Rev. C **59**, 21 (1999).
[22] T. A. Rijken, M. M. Nagels, and Y. Yamamoto, Prog. Theor. Phys. Suppl. **185**, 14 (2010).
[23] T. Ueda, K. Tominaga, M. Yamaguchi, N. Kijima, D. Okamoto, K. Miyagawa, and T. Yamada, Prog. Theor. Phys. **99**, 891 (1998); K. Tominaga, T. Ueda, M. Yamaguchi, N. Kijima, D. Okamoto, K. Miyagawa, and T. Yamada, Nucl. Phys. A **642**, 483 (1998).
[24] M. Danysz, K. Garbowska, J. Pniewski, T. Pniewski, J. Zakrzewski, E. R. Fletcher, J. Lemonne, P. Renard *et al.*, Nucl. Phys. **49**, 121 (1963).
[25] Y. Fujiwara, Y. Suzuki, and C. Nakamoto, Prog. Part. Nucl. Phys. **58**, 439 (2007); Y. Fujiwara, M. Kohno, C. Nakamoto, and Y. Suzuki, Phys. Rev. C **64**, 054001 (2001).
[26] J.-M. Sparenberg and D. Baye, Phys. Rev. C **55**, 2175 (1997)
[27] W. G. Gong, W. Bauer, C. K. Gelbke, and S. Pratt, Phys. Rev. C **43**, 781 (1991).
[28] S. E. Koonin, Phys. Lett. **70B**, 43 (1977).
[29] M. Gyulassy and L. McLerran, Nucl. Phys. A **750**, 30 (2005).
[30] S. Pratt, Phys. Rev. Lett. **102**, 232301 (2009).
[31] O. Hashimoto and H. Tamura, Prog. Part. Nucl. Phys. **57**, 564 (2006).
[32] N. Makhlin and Yu. M. Sinyukov, Z. Phys. C **39**, 69 (1988).
[33] K. Morita, S. Muroya, C. Nonaka, and T. Hirano, Phys. Rev. C **66**, 054904 (2002).
[34] S. Chapman, P. Scotto, and U. Heinz, Heavy Ion Phys. **1**, 1 (1995).
[35] J. D. Bjorken, Phys. Rev. D **27**, 140 (1983).
[36] G. Agakishiev *et al.* (STAR Collaboration), Phys. Rev. Lett. **108**, 072301 (2012).
[37] K. Morita, S. Muroya, H. Nakamura, and C. Nonaka, Phys. Rev. C **61**, 034904 (2000).
[38] S. Pratt, Phys. Rev. D **33**, 1314 (1986).
[39] B. R. Schlei, U. Ornik, M. Plümer, and R. M. Weiner, Phys. Lett. B **293**, 275 (1992).
[40] T. A. Rijken and Y. Yamamoto, Phys. Rev. C **73**, 044008 (2006).
[41] P. Grassberger, Nucl. Phys. B **120**, 231 (1977).
[42] T. Csörgő, B. Lörstad, and J. Zimányi, Z. Phys. C **71**, 491 (1996).
[43] U. A. Wiedemann and U. Heinz, Phys. Rev. C **56**, 3265 (1997).
[44] M. W. Sullivan *et al.*, Phys. Rev. D **36**, 674 (1987).
[45] K. Redlich (private communications).
[46] S. Takeuchi and M. Oka, Phys. Rev. Lett. **66**, 1271 (1991).
[47] S. Cho *et al.* (ExHIC Collaboration), Phys. Rev. C **84**, 064910 (2011); Phys. Rev. Lett. **106**, 212001 (2011).
[48] N. Shah (STAR Collaboration) (private communication).
[49] K. Nakazawa and H. Takahashi, Prog. Theor. Phys. Suppl. **185**, 335 (2010).
[50] C. Amsler *et al.* (Particle Data Group), Phys. Lett. B **667**, 1 (2008).
[51] E. Hiyama, M. Kamimura, Y. Yamamoto, and T. Motoba, Phys. Rev. Lett. **104**, 212502 (2010).
[52] K. S. Myint, S. Shinmura, and Y. Akaishi, Eur. Phys. J. A **16**, 21 (2003).
[53] M. Kohno, Phys. Rev. C **88**, 064005 (2013).